MEDICAL APPLICATIONS AND ENERGY EFFICIENCY OF PRODUCTS OBTAINED FROM NATURAL RESOURCES AND SECONDARY RAW MATERIALS OF GEORGIA

Kh. Barbakadze[1*], E. Tskhakaia[1,2], L. Kvinikadze[1,2], M. Rusia[3], I. Didbaridze[4], B. Arziani[1], N. Lekishvili[3], A. Aliyev[5], G. Tatishvili[2]

[1]Tbilisi State Medical University, Faculty of Pharmacy, Department of Pharmaceutical, Toxicological and Medical Chemistry, 33 V. Pshavela Ave., 0186; Tbilisi, Georgia;
[2]Rafiel Agladze Institute of Inorganic Chemistry and Electrochemistry of Iv. Javakhishvili Tbilisi State University; 11 Mindeli Str., 0186; Tbilisi, Georgia;
[3]Iv. Javakhishvili Tbilisi State University, Faculty of Exact and Natural Sciences, Department of Chemistry; 3 Ilia Tchavtchavadze Ave., 0179 Tbilisi, Georgia;
[4]Akaki Tsereteli State University; 59 Tamar Mepe Str., 4600 Kutaisi, Georgia
[5] Institute of Chemistry, Ministry of Science and Education of the Republic of Azerbaijan, H. Javid 113, AZ 1143, Baku, Azerbaijan
**e-mail: kh.barbakadze@tsmu.edu*

Received 10.03.2026
Accepted 07.06.2026

Abstract. *Fuel cells based on H_2S isolated from Black Sea depth layers have been elaborated. Optimized materials were selected based on electrochemical performance, operational stability, and deactivation resistance. Remarkably, the selected electrode–catalyst exhibited high tolerance to $H_2S$and its oxidation products, showing no significant poisoning effects. Operating under low-temperature conditions, this system eliminates the need for expensive noble-metal catalysts, offering a highly economical and scalable alternative for sustainable energy conversion.*
The pyridine bonded to some transition metals in coordination compounds is one of the most prospective and accessible nitrogen-containing ligands and tetrathioarsenate groups obtained based on the transformation of arsenic industrial waste and natural resources of Georgia have been synthesized and characterized.
Keywords: *Natural and secondary resources, fuel element, arsenic, coordination compounds.*

Introduction

Technical progress based on traditional energy, along with a number of advantages, negatively affects the environment and causes global climate change. At the current stage of development of chemical sciences, the issue of finding new non-traditional energy sources is an important task for both the energy industry and the household sector [1, 2]. As the global demand for sustainable development continues to grow, the search for new and affordable raw materials—derived from secondary resources or responsibly managed natural sources—has become increasingly important [3, 4]. This approach not only reduces production costs but also significantly minimizes environmental pollution caused by industrial waste. By transforming waste into valuable resources, industries can move toward a circular economy that promotes efficiency, innovation, and environmental responsibility. In this regard, Georgia has an interesting potential.

Nowadays, "renewable energy technologies" such as solar, wind, hydrogen, hydroelectric power, biomass, and biofuels for transportation are being widely implemented in many areas of human activity. Among alternative energy sources, hydrogen energy is of particular importance, as it may solve the most pressing environmental problems of large cities in the world in the near future, primarily in terms of air pollution [5]. Accordingly, the search for sources of raw materials for hydrogen and the production of hydrogen or electricity from appropriate raw materials remains a significant challenge.

The critical condition for the transition to hydrogen energy is the creation of economic and ecological fuel cells operating on hydrogen or hydrogen-containing raw materials. Among the hydrogen-containing raw materials used in fuel cells, hydrogen sulfide attracts special attention. In this regard, the Black Sea is an object of scientific attention, since its deep waters contain a large

amount of hydrogen sulfide, hydrosulfide, and sulfide ions (according to various estimates, 4.6-80 billion tons). Their sources of origin are gases erupted from volcanoes and geological cracks on the seabed, organic matter brought by rivers, and decomposition products of microorganisms.

Based on various data, the amount of hydrogen sulfide in the Black Sea increases by 4-9 million tons annually, and its total amount can be estimated at quite significant amounts − 4.6-80 billion tons.

The extraction and use of useful components (for example, H_2S, CH_4, etc.) from seawater as raw materials is of great importance, both for solving the ecological problem of seawater (reducing greenhouse gas emissions into the atmosphere), and for obtaining a non-traditional energy source. When implementing the above-mentioned technological processes, no negative impact on the environment is observed; the salinity and acidity of seawater do not change, there is no imbalance, and no unwanted waste is generated.

Therefore, the aim of this study was to develop and optimize an economical low-temperature fuel cell for the electrochemical conversion of H_2S from the Black Sea, using stable and poisoning-resistant electrode–catalyst materials.

Experimental part

Laboratory and large-scale laboratory models of a fuel cell operating on hydrogen sulfide extracted from the deep waters of the Black Sea have been created. When studying the processes occurring in a fuel cell, many questions arise about the use of thermodynamic ratios, the chemical potential of certain electrodes based on existing data, and the electrochemical action. Today, the use of such complex systems as ion-exchange membranes or modified zeolites in technological processes is very relevant. Analysis of the data obtained as a result of experimental studies of similar systems has shown that the use of simple thermodynamic ratios does not always allow drawing correct conclusions about the processes occurring in such systems.

In this context, analyzing both the classical and quantum-chemical calculations of the thermodynamic parameters governing processes on solid surfaces such as membranes and zeolites is of profound interest [6–9]. Chemical processes occurring in solutions are fundamentally driven by the system's tendency to achieve thermodynamic equilibrium. From a thermodynamic perspective, the change in the Gibbs free energy, dG, during the transition from the initial to the final state serves as the critical criterion for evaluating these systems.

To provide a comprehensive thermodynamic description of a system, it is essential to define its composition, particle concentrations, temperature (T), pressure (P), entropy (S), and volume (V). Accounting for these variables yields the classical differential expression for the Gibbs free energy:

$$dG = - SdT + VdP + \sum_i \mu_i dn_i \qquad (1)$$

where, n_i is the number of moles of the i^{th} component of the system, μ_i and - the chemical potential of the i^{th} component.

For electrochemical systems and fuel cells, the correlation between the Gibbs free energy and the electromotive force (EMF) is of paramount importance. Under isobaric-isothermal conditions (T, P = const), the maximum electrical work generated by a fuel cell is directly determined by the change in the Gibbs free energy:

$$\Delta G=-nFE \qquad (2)$$

where:

- ΔG is the Gibbs free-energy change;
- n is the number of electrons participating in the electrochemical reaction;
- F is the Faraday constant;
- E is the electromotive force (cell voltage).

This fundamental relationship demonstrates that the cell voltage is directly coupled to the thermodynamic driving force of the electrochemical reaction. Consequently, variations in the fuel-cell voltage inherently reflect alterations in the energetic efficiency and electrochemical performance of the fuel H_2S cell.

The experiments were conducted in a fuel cell model manufactured by us, which used an anionic membrane of the Ralex-AM-PP type (dimensions 16 cm x 17 cm), as electrodes, multicomponent metal grids (area 272 cm^2) were used, which, along with the function of the electrode, also play the role of a catalyst. Its composition is (wt. %): Fe – 70; Cr - 17.55; Ni - 9.5; Mn - 1.61; Ti - 0.41, also contains small amounts of V, Nb, Mo, and Cu. The selected electrode-catalyst is not poisoned by hydrogen sulfide and its oxidation products. Background solution - NaCl (27 g/L) + Na_2SO_4 (4 g/L), Na_2S instead of H_2S - converted to hydrogen sulfide (CH_2S = 50, 95, 120, 160, 220 mg/L). The resistance in the external circuit varied from 1000 ohms to 0, the solution was supplied at a rate of 300 ml/hr, or 500 ml/hr, and air was 150 l/hr. During the experiment, all electrical characteristics were measured: current strength (I, mA) and voltage (U, mV), current density (i, mA/cm^2), and power (P, mW).

Methods. IR spectra have been obtained on the spectrometer "SPECORD IR-75" in vaseline oil. X-ray studies were carried out on the diffractometer "ДRON-3M", thermographic studies were carried out on the derivatograph "Q-1500" ("F. Paulik, J. Paulik, L. Erdey", Hungary), by heating the test specimen in the air up to 1000°C at 10°C/min. The reference substance is corundum.

Results and discussion

The present study proposes the use of a fuel cell system for generating electricity from hydrogen sulfide dissolved in the waters of the Black Sea. Hydrogen sulfide, which accumulates in the deep anoxic layers of the Black Sea, represents a substantial and largely untapped chemical energy resource.

In conventional hydrogen sulfide decomposition processes, elemental sulfur is typically produced as the final product. However, from an electrochemical perspective, the formation of elemental sulfur involves the transfer of only two electrons per molecule of hydrogen sulfide oxidized. In contrast, within a fuel cell configuration, it is thermodynamically and energetically more advantageous to oxidize sulfide ions to sulfate ions at the anode (Figure 1). This anodic reaction involves the transfer of eight electrons per sulfide species, thereby enabling the generation of four times more electrical energy compared to the two-electron pathway leading to elemental sulfur.

Accordingly, the proposed fuel cell approach not only facilitates efficient energy recovery from hydrogen sulfide but also enhances the overall energy yield through the eight-electron oxidation mechanism, offering a promising strategy for sustainable power generation.

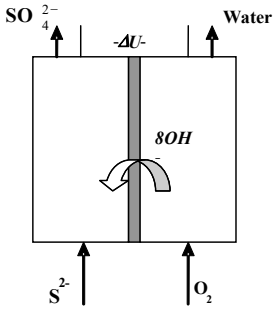

Fig. 1. Schematic representation of the process proceeding in a fuel cell

$$S^{2-} + 8OH^- \rightarrow SO_4^{2-} + 4H_2O + 8\bar{e} \quad (A)$$

$$2O_2 + 4H_2O + 8\,\bar{e} \rightarrow 8OH^- \quad (K)$$

Membranes (Ralex-AM-PP) for fuel cells were selected, and processes passing on certain electrodes of the fuel cell were studied. Figure 2 illustrates the polarization behavior of the H_2S fuel cell. The operational current and voltage values were experimentally recorded, while the current density and power output were subsequently calculated with respect to the geometric (visible) surface area of the electrode. The recorded current–voltage characteristics exhibit a characteristic progressive decline in cell voltage as the current density increases. The open-circuit voltage (OCV) reaches approximately 901 mV, confirming the successful thermodynamic and electrochemical initiation of the system. As the current demand scales up to ~10 mA the cell voltage drops significantly to the range of 70–100 mV, a phenomenon primarily attributed to activation polarization, mass transport limitations, and internal ohmic resistance. Notably, the relatively smooth profile of the voltage decay underscores the stable operational performance of the fuel cell under the investigated experimental conditions. While these initial electrochemical metrics are promising for a preliminary H_2S fuel cell configuration, substantial optimization regarding electrode architecture, catalyst materials, and operating parameters remains imperative. Addressing these factors will be crucial to mitigating polarization losses, reducing internal resistance, and ultimately maximizing the net power density output.

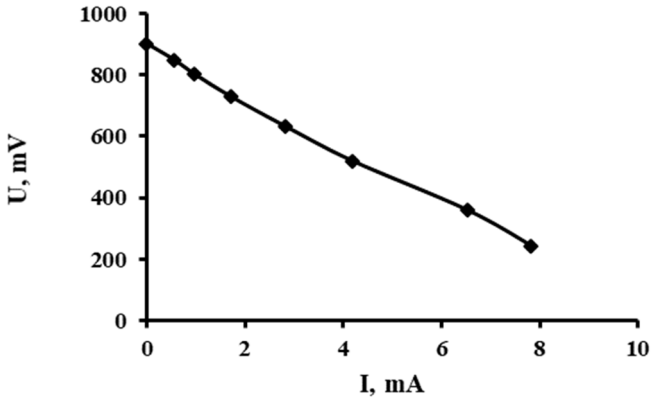

Fig. 2. Polarization behavior of the H_2S fuel cell

Studies have shown that at low H_2S concentrations (50 mg/l), increasing the solution delivery rate (from 300 ml/h to 500 ml/h), practically does not change the capacity, while at high concentrations (150 mg/l and 220 mg/l) it increases by 50-80% (Fig. 2).

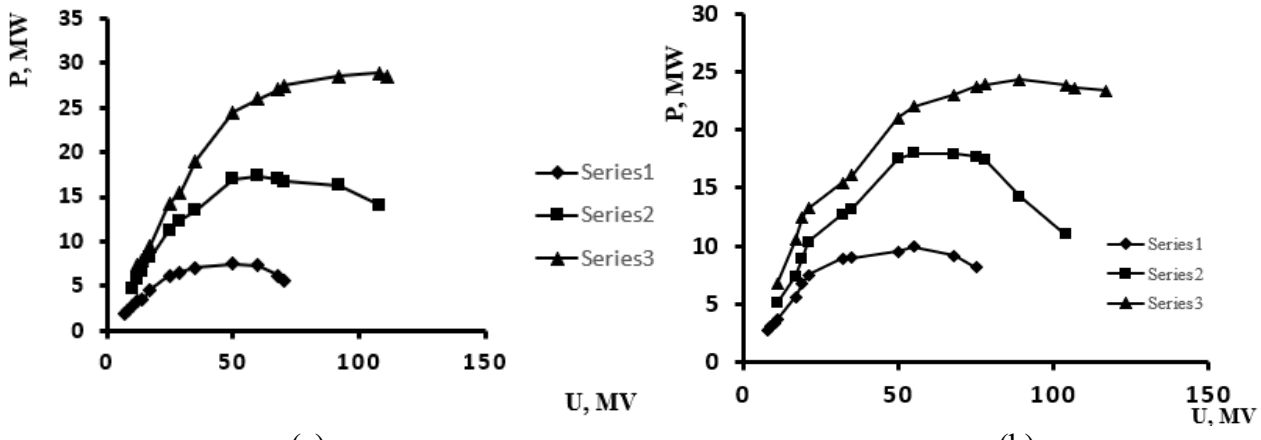

(a) (b)

Fig. 3. Power characteristics of the H_2S-fueled cell: Dependence of cell power (P, mW) on cell voltage (U, mV) across three different concentrations of hydrogen sulfide – 1- 50 mg/L; 2 - 150 mg/L; 3 - 220 mg/L; Solution supply rate - 300 ml/h (a) and 500 ml/h (b)

Fig. 3 displays the comparative power characteristics (P-U curves) of the H_2S fuel cell system across three distinct experimental conditions (Series 1, 2, and 3) under two different operational

modes, designated as (a) and (b). In all evaluated profiles, the power output exhibits a classic non-linear dependence on the cell voltage; it progressively ascends to a maximum peak (maximum power point) before undergoing a downward trajectory due to severe polarization losses and internal mass transport limitations at specific voltage thresholds.

Taken together, the experimental data indicate that the electrochemical performance of the H_2S fuel cell is governed by a synergistic interplay between reactant concentration and volumetric flow rate. At low concentrations (Series 1), the system is strictly mass-reactant limited, exhibiting minimal sensitivity to flow rate adjustments. Conversely, at higher concentration thresholds, optimizing the flow rate is critical; excessive delivery rates (mode b) reduce the maximum power output of Series 3 from 29 mW to 24.5 mW, likely due to shortened reactant residence times or localized electrode flooding. Additionally, the abrupt power drop-off in Series 2 (Fig. 3b) past 75 mV highlights severe mass transport and diffusion constraints under accelerated flow regimes. These insights successfully correlate with the proposed thermodynamic framework, proving that precise regulation of chemical potential and mass transport kinetics is essential to maximize the system's net energetic efficiency.

Arsenic-containing industrial waste generated in Georgia represents a potentially valuable secondary raw material for the synthesis of a range of commercially and scientifically significant compounds. Such waste streams may serve as precursors for the recovery of gold and for the production of various arsenic-based compounds, including barium hydrous arsenate, strontium hydrous arsenate, magnesium–ammonium arsenate, sodium monoselenoarsenate, and cyclic esters of arsenic acid.

Among these products, barium hydrous arsenate has been reported as an effective anthelmintic agent. Strontium hydrous arsenate finds application in homeopathy and is also used in veterinary medicine as an anthelmintic. Magnesium–ammonium arsenate is utilized in the manufacture of specialty glasses, while sodium monoselenoarsenate is employed as an insecticide. Cyclic esters of arsenic acid have broader industrial relevance, being used in the formulation of insecticides, as oxidation inhibitors in lubricants, as antioxidants for synthetic rubber, and in the production of certain copolymers.

Homeopathy, as a distinct and increasingly discussed therapeutic approach, has attracted renewed scientific and clinical interest in recent years. Within this context, selected arsenic compounds derived from industrial waste may offer promising opportunities for further investigation and application.

The development of these directions would contribute to the establishment of a cost-effective raw material base, facilitating both the production of well-known arsenic-containing compounds and the synthesis of novel derivatives with potentially valuable properties. Such an approach would enhance the feasibility of their practical implementation (Scheme 1) [10, 11].

Under conditions of limited primary resources, the transformation of arsenic-containing production waste into coordination compounds with specific and potentially useful properties represents a strategically important objective. This approach not only enables the development of commercially attractive chemical forms but also addresses a critical environmental challenge by reducing arsenic-related contamination. In particular, the synthesis of new bioactive coordination compounds from arsenic-containing waste appears to be one of the most promising pathways for simultaneously achieving economic and environmental benefits.

Polyelement coordination compounds manifest a lot of interesting properties that give an opportunity for their wide practical application. In recent years, the coordination compounds containing tetrathioarsenate groups and nitrogen and d-metals have attracted particular interest [10-13].

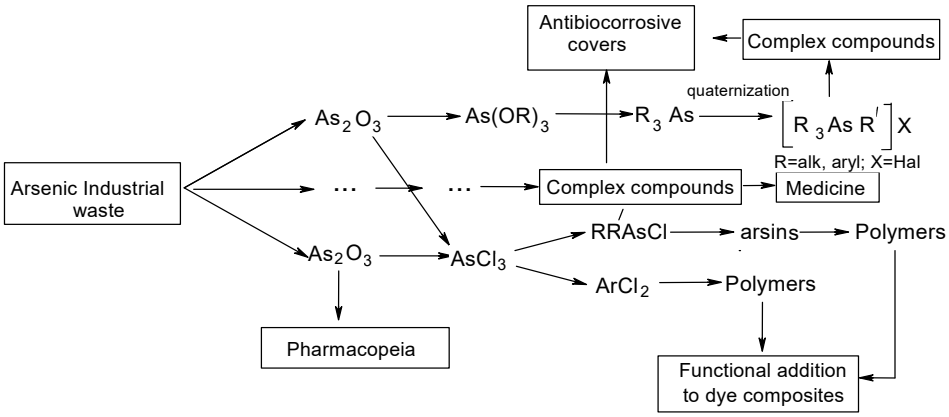

Scheme 1. The obtaining and use of important arsenic-containing compounds from arsenic industrial waste

The goal of our research is to obtain and study coordination compounds of zinc, mercury (II), copper (II), and nickel (II) with pyridine, one of the most prospective and accessible nitrogen-containing ligands received on the basis of products obtained via transformation of the abovementioned production waste. These compounds may manifest high bioactivity.

As the initial compounds, we have used zinc acetate, mercury(II) nitrate, copper(II) sulfate, and nickel(II) chloride, i.e., salts of the aforementioned metals soluble in water. Among arsenic-containing compounds, we have used sodium tetrathioarsenate $Na_3AsS_4 \cdot 8H_2O$, which we received using processing of arsenic production waste (Scheme 2) [14, 15]:

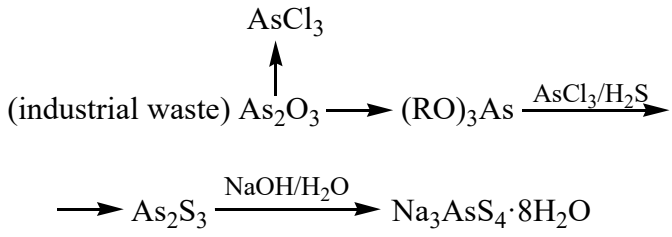

Scheme 2

Synthesis of d-metal pyridinates proceeds according to the following reaction (Scheme 3):

$$3MX_2 + 3nC_5H_5N + 2Na_3AsS_4 \cdot 8H_2O \rightarrow [M(C_5H_5N)_n]_3(AsS_4)_2\downarrow + 6NaX + 16H_2O$$

Scheme 3

Obtained coordination compounds represent solid, colored, finely crystalline substances, which are well soluble in dimethylformamide but are not dissolved in water, alkali, ethyl spirits, liquid saturated hydrocarbons, and are disintegrated at high temperatures up to melting. During acid treatment, they experience a transformation with the formation of arsenic(V) sulfide:

$$[Zn(Py)_4]_3(AsS_4)_2 + 6HCl \rightarrow 3[Zn(Py)_4]Cl_2 + As_2S_5 + 3H_2S$$

Scheme 4

The composition and structure of the obtained compounds were established by means of data from element analysis (Table 1), infrared spectroscopy, and X-ray phase studies.

As is seen from the IR spectra of the synthesized compounds, valence vibration absorption bands, which are characteristic of AsS_4^{3-} group, are manifested in them at 420 cm^{-1}, while absorption bands of deformation vibration are at 470 cm^{-1} [16]. Besides, as is known [17], the value of the absorption band during the free ligand's coordination with the central atom experiences a shift of ~8-30sm^{-1}. The absorption band of uncoordinated pyridine υ(C=N) is located in the 1580 cm^{-1} area [17],

while the same absorption band in spectra of compounds synthesized by us is manifested in the 1600-1610 cm^{-1} area that unequivocally confirms the existence of pyridine coordinated with metal ions in these compounds.

Table 1. Elemental analysis data and output of the synthesized $[M(Py)_n]_3(AsS_4)_2$-type complex compounds

№	Formula complex compounds	Color	Date of elemental analysis Calculated/found, %				The yeald, %
			M	As	N	S	
I	$[Cu(C_5H_5N)_4]_3(AsS_4)_2$	grey	12.33 / 12.11	9.71 / 9.94	10.87 / 10.64	16.57 / 16.71	93.4
II	$[Zn(C_5H_5N)_4]_3(AsS_4)_2$	light yellow	12.64 / 12.77	9.67 / 9.49	10.83 / 10.58	16.51 / 16.69	96.5
III	$[Cd(C_5H_5N)_4]_3(AsS_4)_2$	carroty	19.22 / 20.02	8.87 / 8.81	9.93 / 9.84	15.13 / 15.26	95.3
IV	$[Hg(C_5H_5N)_4]_3(AsS_4)_2$	grey	30.77 / 29.89	7.66 / 7.85	8.58 / 8.23	13.08 / 13.02	95.2
V	$[Ni(C_5H_5N)_6]_3(AsS_4)_2$	black	8.82 / 9.19	7.48 / 7.71	12.56 / 12.32	12.76 / 12.51	92.8

Very close agreement of tetrathioarsenate-ion absorption bands with the absorption bands of sodium tetrathioarsenate-ions indicates the fact that the mentioned anion creates a second sphere of coordination compound. Data of X-ray phase analysis of synthesized substances (Table 2), based on classification given in the literature [18], testifies that obtained compounds, according to their structural nature, belong to the subgroup of sulfosalts. Cations' impact on ordering of crystal structure deserves special attention. For example, copper (II) and mercury (II) promote the formation of a finely crystalline phase, which approaches the X-ray amorphous state [19].

At the initial stage, a breakaway of the ligand from the complex compound's molecule takes place, and afterwards, stage-by-stage thermal decomposition of tetrathioarsenate (V) continues [20].

Table 2. Roentgenphase analysis data of tetrathioarsenates(V) of pyridine complex with some d-metals

$[Cu(Py)_4]_3(AsS_4)_2$		$[Cd(Py)_4]_3(AsS_4)_2$		$[Ni(Py)_6]_3(AsS_4)_2$		$[Hg(Py)_4]_3(AsS_4)_2$	
I/I_0	D α/n	I/I_0	d α/n	I/I_0	d α/n	I/I_0	D α/n
20	11.33	20	13.0	2	11.0	4	11.6
100	8.19	15	9.07	3	7.86	2	7.69
20	7.23	10	7.0	3	6.81	2	7.26
20	6.56	25	6.41	4	6.34	5	6.10
10	5.71	15	5.96	5	5.43	5	5.62
10	5.33	10	4.33	4	4.76	6	5.00
10	5.07	35	3.90	3	3.81	8	4.73
20	4.38	25	3.27	6	3.58	10	4.62
20	4.04	15	3.17	2	3.27	7	4.33
15	3.87	15	3.05	3	2.98	9	3.92
5	3.24	20	2.98	10	2.82	3	3.75
5	3.16	20	2.94	3	2.56	3	2.82
5	3.00	15	2.43	2	2.51	3	2.46
5	2.95	30	2.23	3	2.25	2	2.18
5	2.75	30	2.19	2	2.19	2	2.04
8	2.53	20	2.15	3	2.12	3	1.93
5	2.44	10	2.08	4	1.98	3	1.86
10	2.11	15	1.97	3	1.86		
10	1.97	15	1.94				
10	1.92	40	1.83				
		100	1.77				

As is seen from results of thermographical study, processes of thermal decomposition (thermolysis) of complex compounds of copper and zinc are almost similar (Fig. 4).

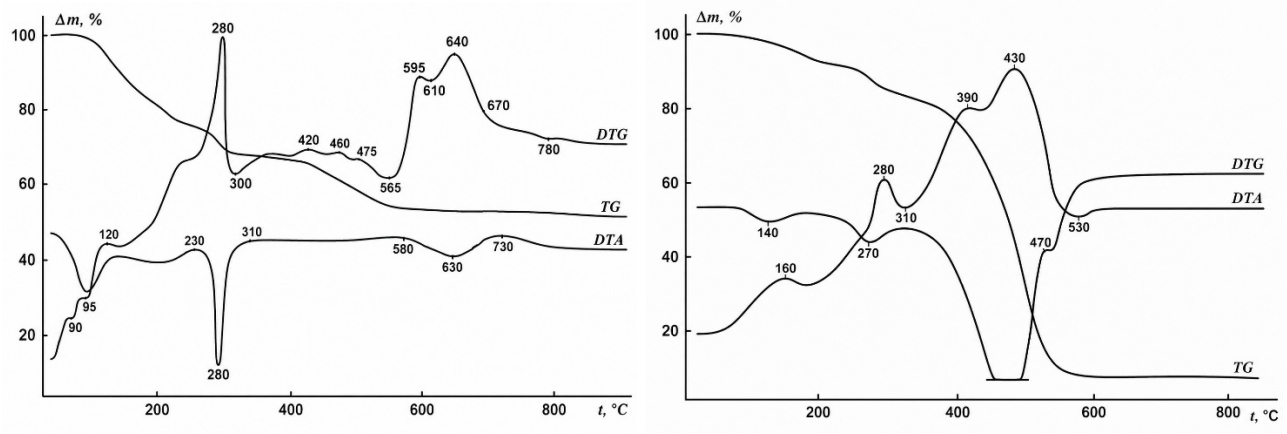

(a) (b)

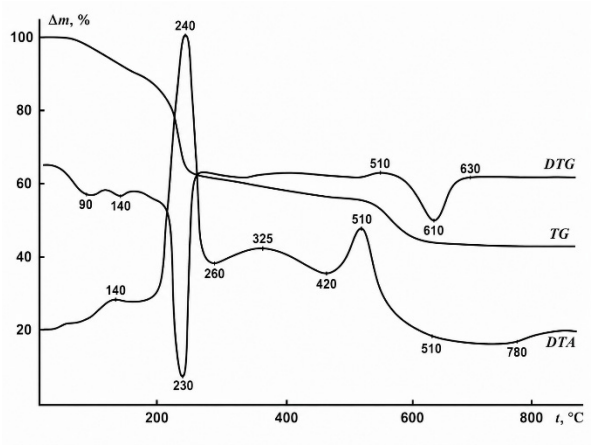

(c)

Fig. 4. Thermogravimetric graphs of synthesized compounds: a) $[Zn(Py)_4]_3(AsS_4)_2$; b) $[Hg(Py)_4]_3(AsS_4)_2$; c) $[Ni(Py)_6]_3(AsS_4)_2$

The obtained complexes are showing two types of thermal decomposition (Scheme 5 and 6):

$$[Ni(Py)_6]_3(AsS_4)_2 \xrightarrow[-6Py]{100-200^0C} [Ni(Py)_4]_3(AsS_4)_2 \xrightarrow[-12Py]{200-240^0C} Ni_3(AsS_4)_2 \xrightarrow[-3S]{250-420^0C}$$

$$\xrightarrow[-3S]{250-420^0C} Ni_3AsS_5\,(3MS{\cdot}As_2S_2) \xrightarrow[-AS_2S_2]{420-920^0C} 3MS$$

Scheme 5. Thermolysis of nickel tetrathioarsenate (V) pyridine complex

$$[Hg(Py)_4]_3(AsS_4)_2 \xrightarrow[-6Py]{100-200^0C} [Hg(Py)_2]_3(AsS_4)_2 \xrightarrow[-6Py]{200-240^0C} Hg_3(AsS_4)_2 \xrightarrow[-2S]{240-330^0C}$$

$$Hg_3As_2S_6 \xrightarrow[-2Hg]{330-430^0C} HgAs_2S_6 \xrightarrow[-HgS,-As_2S_5]{>430^0C} \text{full decomposition}$$

Scheme 6. Thermolysis of mercury (II) tetrathioarsenate (V) pyridine complex

Thermolysis of the $[Ni(Py)_6]_3(AsS_4)_2$ sample (Fig. 4c) begins from 100°C. Gravimetric analysis showed that the first 6 moles of ligand break away at 200°, which corresponds with 23.0% of weight loss (theoretically 23.6%). In the range of 200-250°C, a very important endothermal effect is

observed, with a minimum at 235°C. The other 12 moles of ligand break away in this interval. Therefore, the sample's weight loss is 46% (theoretically 47.28%). Since then, thermal decomposition of the sample continues in the same way as in the case of the corresponding neutral salt.

As is seen from the comparison of diagrams, the thermal decomposition of the pyridine complex of Hg(II) tetrathioarsenate(V) $\{[Hg(Py)_4]_3(AsS_4)_2\}$ must occur in a different way. Ligand breakaway can also be represented step by step here: at the first step, in the range of 100-200°C, the complex loses 6 moles of pyridine, while the other 6 moles are lost in the range of 200-240°C. Weight loss at both stages is equal to 31% (theoretically 30.77%). After the ligand's breakaway, the process of thermal decomposition continues in the same way as in the case of the corresponding neutral salt [20].

Along with thermogravimetric analysis data obtained results are confirmed by the processes of thermal decomposition of intermediate products, which is described in literature, as well as by analysis of composition of residues formed at the various stages [15-20].

Using the method of density functional theory, the total energy of tetrahedral complex ions $[Zn(C_5H_5N)_4]^{2+}$, $[Cd(C_5H_5N)_4]^{2+}$, $[Hg(C_5H_5N)_4]^{2+}$, $[Cu(C_5H_5N)_4]^{2+}$ (Scheme 6) and rows of metal-nitrogen bonds in them (Table 3) were calculated. For the estimation, a basis with pseudopotential (only valence electrons) is used, which implies relativistic corrections.

Table 3. Total energy of tetrahedral complex ions and rows of metal-nitrogen bonds in them

Ion	Full energy, kJ/mol	Bond order			
		N_1	N_2	N_3	N_4
Zn^{2+}	-1026272.49	0.47	0.47	0.47	0.47
Cd^{2+}	-870624.67	0.35	0.35	0.35	0.35
Hg^{2+}	-836100.01	0.36	0.36	0.36	0.36
Cu^{2+}	-948390.59	0.54	0.54	0.54	0.54

Theoretical estimation of bioactivity of metal-pyridine fragments of obtained coordination compounds has been carried out using computer program PASS C&T [21], which is performed by P_a (active) and P_i (inactive) parameters. Prior to that, Na_3AsS_4 was calculated, which manifested antiprotozoal (Amoeba) and antihelminthic (Nematodes, Fasciola) activity of P_a=0.507-0.898. Calculations show that the metal-pyridine fragment of the synthesized coordination compound, presumably, also manifests high bioactivity. Selected structures with high probability (P_a=0.570-0.900) (Table 4) may manifest the following kinds of biological activity: Atherosclerosis treatment, Antineoplastic, antiseborrheic, antiviral picornavirus, cytoprotectant, etc.

Table 4. The results of calculated virtual bioactivity of metal-pyridine fragments of tetrathioarsenates(V) some of d-metals

Compound	Atherosclerosis treatment	Antineoplastic	Anemia, sideroblastic	Antiseborrheic	Antiviral (Picornavirus)	Cytoprotectant	Antineurotic	Insulin promoter
	P_a / P_i							
$[Cu(C_5H_5N)_4]_3(AsS_4)_2$	-	-	0.874/0.002	0.870/0.007	0.666/0.009	0.655/0.013	0.679/0.046	0.625/0.012
$[Zn(C_5H_5N)_4]_3(AsS_4)_2$	0.991/0.002	0.892/0.005	0.859/0.003	0.852/0.010	0.639/0.012	0.637/0.018	0.624/0.063	0.570/0.018
$[Cd(C_5H_5N)_4]_3(AsS_4)_2$	0.987/0.002	0.953/0.004	0.822/0.004	0.852/0.010	0.583/0.023	0.598/0.031	0.624/0.063	0.570/0.018
$[Hg(C_5H_5N)_4]_3(AsS_4)_2$	0.987/0.002	0.953/0.004	0.852/0.010	0.852/0.010	0.563/0.023	0.578/0.031	0.624/0.063	0.563/0.018
$[Ni(C_5H_5N)_6]_3(AsS_4)_2$	-	0.945/0.004	0.867/0.003	0.839/0.012	0.574/0.025	0.602/0.030	0.601/0.071	0.579/0.025
$[Co(C_5H_5N)_6]_3(AsS_4)_2$	-	-	0.859/0.003	0.886/0.005	0.645/0.011	0.640/0.017	0.725/0.034	0.673/0.008

Conclusions

Laboratory-scale and pilot-scale fuel cell models were designed and constructed. Their performance was systematically investigated using various electrode materials. Particular attention was devoted to identifying electrode systems capable of functioning both as conductive elements and as effective electrocatalysts. The most efficient electrode–catalyst materials were selected based on electrochemical performance, stability, and resistance to deactivation. Notably, the selected electrode–catalyst demonstrated high tolerance to hydrogen sulfide and its oxidation products, showing no significant poisoning effects. The overall process operates under low-temperature conditions and is economically advantageous, as it eliminates the need for expensive and complex noble-metal catalysts.

In parallel, coordination compounds of the general formula $[M(Py)_n]_3(AsS_4)_2$ (where M represents a d-metal and Py denotes pyridine) were synthesized using transformation products derived from arsenic-containing industrial waste and natural resources of Georgia. The composition and structural features of the obtained compounds were established through comprehensive physicochemical characterization methods.

Theoretical evaluation of their potential biological activity was performed using specialized computational modeling software. The calculated virtual bioactivity results indicate that the conjugation of metal–pyridine fragments with tetrathioarsenate units represents a promising strategy for the design of a broad range of coordination compounds exhibiting potential antimicrobial and anthelmintic properties.

References

1. AL-Jubouri R.J.N., Jabrail F.H. Chemical characterization of eco-friendly recovery method for rubber from waste tires. *Chemical Problems,* 2024, **Vol. 22(4)**, p. 458-467. DOI: 10.32737/2221-8688-2024-4-458-467
2. Terlouw T., Rosa L., Bauer Ch., McKenna R. Future hydrogen economies imply environmental trade-offs and a supply-demand mismatch. *Nature Communication,* 2024, **Vol. 15**, 7043. DOI: 10.1038/s41467-024-51251-7
3. Alenezi M., Alarbeed B., Alqaheem Y. Metal hydrides and metal-organic frameworks for hydrogen storage in automotive applications: A review. *Chemical Problems,* 2024, **Vol. 22(1)**, p. 76-94. DOI: 10.32737/2221-8688-2024-1-76-94
4. Awadh Kh., Al-Qaheem Y. Hydrogen generation using low carbon technologies. *Chemical Problems,* 2023, **Vol. 21(4)**, p. 307-322. DOI: 10.32737/2221-8688-2023-4-307-322
5. Maka A.O.M., Alabid J.M. Solar energy technology and its roles in sustainable development. *Clean Energy*, 2022, **Vol. 6(3)**, p. 476–483. DOI: 10.1093/ce/zkac023.
6. Zha X., Li F., Feng B., Zhang X., He R. Adsorption Mechanism and Regeneration Performance of Calcined Zeolites for Hydrogen Sulfide and Its Application. *ACS Omega*, 2024, **Vol. 9(17)**, p. 19493–19503. DOI: 10.1021/acsomega.4c00987
7. Marsagishvili T., Ananiashvili N., Metreveli J., Tatishvili G., Tskhakaia E., Tskhakaia E., Khositashvili R. Application of Georgian zeolites for the extraction of useful components from natural and waste waters. *Eur. Chem. Bull.,* 2014, **Vol. 3(1)**, p. 102-103. DOI:10.48616/openscience-584
8. Morales-García A., Viñes F., Sousa C. Toward a Rigorous Theoretical Description of Photocatalysis Using Realistic Models. *Journal of Physical Chemistry Letters*, 2023, **Vol. 14 (15)**, p. 3712–37202 DOI: 10.1021/acs.jpclett.3c00359
9. Marsagishvili T., Machavariani M., Tatishvili G., Ckhakaia E. Thermodynamic Analysis of Processes with the Participation of Zeolites. *Bulgarian Chemical Communications,* 2014, **Vol 46(2)**, p. 423-430. DOI:10.48616/openscience-582
10. Deokar P., Leitz D., Stein T.H., Vasiliu M., Dixon D.A., Christe K.O., Haiges R. Preparation and Characterization of Antimony and Arsenic Tricyanide and Their 2,2′-Bipyridine Adducts.

Chemistry – A European Journal, 2016, **Vol. 22(37)**, p. 13251-13257. DOI: 10.1002/chem.201602436
11. Ali S., Bakhtiar S.U.H., Ismail A., Ismail P.M., Hayat S., Zada A., Wu X., Alodhayb A.N., Zahid M., Raziq F., Yi J., Qiao L. Transition metal sulfides: From design strategies to environmental and energy-related applications. *Coordination Chemistry Reviews*, 2025, **Vol. 523**, 216237. DOI: 10.1016/j.ccr.2024.216237
12. Samkharadze M., Rusia M., Barbakadze Kh., Kakhidze N., Pachulia Z., Gigauri R., Lekishvili N. Bioactive Complex Compounds Based on Transition Metals and some Nitrogencontaining Ligands: Synthesis, Structure and Properties. *Oxid. Commun.* 2012, **Vol. 35(3)**, p. 633-650.
13. Didbaridze I., Khelashvili G., Rusia M., Endeladze N. Sodium Tetrathioarsenate as a precipitate of ommoniate ions of Transitional Metals. *Proceedings of the Georgian Academy of Sciences.* 1998, **Vol. 157(2)**, p. 238-240. DOI:10.11648/j.earth.s.2015040501.26
14. Brauer G.M. *Guidance on the inorganic chemistry*. 1985. «MIR». 2. 126-127 p.
15. Didbaridze I., Lekishvili N., Gvetadze L., Bregadze N. Coordination Compounds of some d-metals of tetrathioarsenates (V) with ortho-phenylenediamine. *Web of Scholar,* 2018, **Vol. 1(19),** p. 4-6.
16. Nakamoto K. *Infrared spectra of inorganic and coordination compounds*. 1966. "MIR". 411 p.
17. Shagidulin P.P., Izosimova I. (As=S) in IR and KR Spectra. 1976, *Izvestia of the Academy of Sciences of USSR.* Chem. Serie. **Vol. 5, I,** 863.
18. Belami L. *Infrared spectra of difficult molecules*. 1963. Leningrad. «Inostr. Liter.». 591 p.
19. Lipson G., Stipl G. *Interpretation of Pouder Roentgenogrames*. 1972. "MIR". **Vol. 2**, 384 p.
20. Sadim A., Lagunin A., Filiminov D., Poroikov V. Internet-System of Prognose of the Spectrum of Bioactivity. *Chem. Comp. Chem.-Farm. J.* 2002, **Vol. 36(10)**, p. 21-26. DOI:10.1080/10629360310001623935
21. Nazari A.M., Radzinski R., Ghahreman A. Review of arsenic metallurgy: Treatment of arsenical minerals and the immobilization of arsenic. *Hydrometallurgy*, 2017, **Vol. 174**, p. 258–281. DOI: 10.1016/j.hydromet.2016.10.011